Proceedings of ASME Turbo Expo 2022
Turbomachinery Technical Conference and Exposition
GT2022
June 13-17, 2022, Rotterdam, The Netherlands

GT2022-82438

DESIGN OF AN AIR-COOLED CONDENSER FOR CO2-BASED MIXTURES: MODEL DEVELOPMENT, VALIDATION AND HEAT EXCHANGE GAIN WITH INTERNAL MICROFINS

Viktoria Illyés
TU Wien
Vienna, Austria

Ettore Morosini
Politecnico di Milano
Milan, Italy

Michele Doninelli
University of Brescia
Brescia, Italy

Pierre-Luc David
Kelvion Thermal Solutions
Nantes, France

Xavier Guerif
Kelvion Thermal Solutions
Nantes, France

Andreas Werner
TU Wien
Vienna, Austria

Gioele Di Marcoberardino
University of Brescia
Brescia, Italy

Giampaolo Manzolini
Politecnico di Milano
Milan, Italy

ABSTRACT

CO_2 blends provide tremendous advantages when used as a working fluid in transcritical power cycles with respect to pure CO_2. The benefits become especially apparent if coupled with concentrated solar power since increasing the critical temperature of the blend with respect to pure CO_2 allows dry condensing at high ambient temperatures in locations of high solar radiation. One key cycle component is the cooler, which in this work is designed as an air-cooled condenser with a MATLAB in-house code. The internal, condensation heat transfer model used in this paper relies on a correlation developed by Cavallini (2006). The model itself is validated against experimental data from a test rig for heat transfer measurements on a CO_2 + R1234ze(E) mixture. The resulting design of the condenser is compared with the commercial software HTRI for a specific case study which is representative of the condenser of a recuperated cycle working with a CO_2 + C_6F_6 blend. The authors also present an upgraded heat exchanger design with microfinned tubes, the DIESTA tubes, and groovy fins on the air side. The design of the heat exchanger adopting the mixture is compared to a case with pure CO_2 as the working fluid.

Keywords: Transcritical Rankine cycle, dry-cooling, heat exchanger model, CO_2-based mixtures

NOMENCLATURE

AR	Ratio between external and internal heat exchange area of the condenser
CR	Ratio between minimum and maximum heat capacity of the flow
CSP	Concentrated solar power
$c_{p,v}$	Specific heat capacity of the vapor phase
d	Tube diameter of the heat exchanger
ΔT_{gl}	Temperature glide along isobaric condensation
ΔH_m	Enthalpy difference of isobaric condensation
h	Specific enthalpy
h_c	Convective heat transfer coefficient of pure fluid
$h_{conv,mix}$	Convective heat transfer coefficient of a condensing mixture
h_{loc}	Experimental, local heat transfer coefficient
h_v	Vapor phase heat transfer coefficient
HTC	Heat transfer coefficient
l	Axial length of the tube
$\dot{m}$	Mass flow rate
NTU	Ratio between the product of overall heat transfer coefficient with the area and the minimum heat capacity of two flows in a heat exchanger
$\dot{Q}$	Transferred heat
$\dot{q}$	Heat flux per meter
R_a	Bell and Ghaly resistance
T	Temperature
U	Overall heat transfer coefficient
$\dot{V}$	Volumetric flow rate
x	Vapor fraction
ϵ	Effectiveness of the cross-flow heat exchanger
λ_{steel}	Thermal conductivity of carbon steel
$\eta_{c,CO2}$	Critical viscosity of pure CO_2
$\eta_{Surf,Fin}$	Fin surface efficiency
ρ	Density

Subscripts

loc	Local
w	Wall, measurement position
ext, o	External, out
int	Internal
$cell$	Discretized element in heat exchanger model
in	Inlet of test-tube, measurement position
out	Outlet of test-tube, measurement position
wf	Working fluid

1. INTRODUCTION

Concentrated solar power (CSP) is becoming one of the key renewable energy technologies of the future. Beside its great abundance in nature, solar power has the most significant potential of all renewable energy sources to increase energy supply since the dispatchability of power production has increased due to easy solutions for thermal energy storage.

Currently, a significant part of the scientific research is conducted on innovative power cycles to increase the conversion efficiency and reduce costs [1]. A promising concept is the coupling of CSP plants with a power block working with supercritical carbon dioxide (sCO_2) as working fluid reaching very high temperatures, thus, improving the cycle efficiency. Moreover, the working fluid´s high density throughout the process allows for compact turbomachinery components and lower costs than a conventional steam Rankine cycle.

Nevertheless, the cycle efficiency of sCO_2 cycles is penalized by high cycle minimum temperatures due to the significant compression work. An interesting solution to overcome this hurdle are CO_2-based working fluids (binary mixtures of mainly CO_2 and an additive) to increase the critical temperature of the mixture with respect to pure CO_2 while keeping the advantages of sCO_2 cycles when compared to steam Rankine cycles.

Raising the critical temperature of the working fluid makes its condensation possible at higher temperatures, enabling dry cooling with ambient air in potential CSP-areas, while strongly reducing the compressibility of the pumped flow, adopting a pump instead of a compressor to operate in a liquid subcritical region. The simpler layout and liquid compression reduce costs even further. Besides costs, it has been shown that cycles with CO_2-based mixtures present higher thermomechanical efficiencies than the reference CO_2 cycle [2].

The exploitation of CO_2-based mixtures as working fluids is studied and detailed within the SCARABEUS[1] project, an EU H2020 project with the target of reducing the levelized cost of electricity of CSP plants below 96 €/MWh_{el} adopting the innovative working fluids. Crespi et al. [3] found the following at a maximum temperature of 550 °C and a high pressure of 250 bar for the promising candidates hexafluorobenzene C_6F_6, titaniumtetrachloride $TiCl_4$ and sulfur dioxide SO_2: pure CO_2 and the mixture CO_2-SO_2 with a molar fraction of 30 % SO_2 show the best performance when operated in a *Recompression* cycle, leading to thermal efficiencies of 42.7 % and 45.0 %, respectively. With a C_6F_6 molar fraction of 15 %, the *Precompression* cycle shows a thermal efficiency of 43.6 %. When using $TiCl_4$, a molar fraction of 17 % in the *Recuperated Rankine* cycle performs best, resulting in a thermal efficiency of 45.7 %. Morosini et al. [4] investigated the performances of CO_2+SO_2 mixtures at 700 °C: they found that the optimal molar composition is 15 % SO_2 and the recompression cycle is the most efficient layout, having a cycle efficiency of 50.8 %, 2.1 pp. higher than the respective sCO_2 cycle.

To assess the performance of power cycles - especially in off-design conditions - easy to use and to adapt heat exchanger models are vital. This fact becomes evident especially when large amounts of cycle layouts and working fluids need to be assessed, and the design of the critical components, one of which the condenser is, might have to be adjusted for every set of conditions to perform the further analysis.

In this paper, the authors present a model to design air-cooled condensers of power cycles working with mixtures. Moreover, a comparison with a commercial software is shown for the mixture CO_2 + C_6F_6 for a specific use case. The influence of enhanced tubes on the heat transfer on both the air and working fluid side is discussed.

For the type of condenser, direct cooling with mechanical draft is chosen. The small condenser footprint is in line with the other components of CO_2 or CO_2-based cycles. The scope of the work is hence to develop a comprehensive, detailed and accurate model to design condensers for CO_2-based mixtures power cycles and compare the results with a sCO_2 cooler.

Finally, an experimental validation of the heat transfer coefficient (HTC) correlations for condensing mixtures adopting a representative mixture (CO_2+R1234ze(E)) allows filling the gap in the literature regarding experimental HTC data in the two-phase region of CO_2-based mixtures.

2. METHODS

2.1 Heat exchanger model

The full-scale air-cooled condenser is modelled in MATLAB as a cross-flow heat exchanger with fins on the air side to increase the heat transfer area. In the analysis many different tube layouts are studied: among them, there are the two extreme conditions reported in Fig. 1. In the first layout the flow is not split and the pressure drops are dominant, in the second one, the flow is split twice to minimize the pressure drops. The first layout employs tubes with 7 passes and 7 rows, while in the second one, the tubes have 3 passes and 7 rows. The main characteristics of the tubes and the fins are reported in Tab. 1.

In the code, each row is discretized in 20 cells (and 21 nodes): for each cell the overall heat transfer coefficient U is computed, relative to the external area, accounting both the effects of internal and external convective resistance, along with the conductive one, according to Eq. (1).

[1]Supercritical CARbon dioxide/Alternative Blends for Efficiency Upgrade of Solar power plants; https://www.scarabeusproject.eu/

$$U = \left[\frac{1}{h_{int} \cdot AR} + ln\left(\frac{d_{ext}}{d_{int}}\right) \cdot \frac{d_{int}}{2 \cdot \lambda_{steel} \cdot AR} + \frac{1}{h_{ext} \cdot \eta_{Surf,Fin}}\right] \quad (1)$$

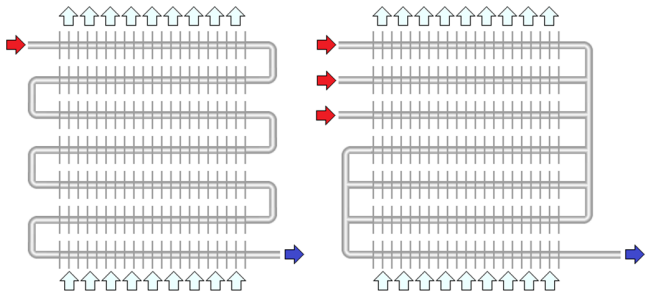

FIGURE 1: TUBE LAYOUTS. LEFT: 7 PASSES AND 7 ROWS, RIGHT: 3 PASSES AND 7 ROWS.

Where the internal convective coefficient is computed according to Cavallini's model [5], while the external convective coefficient according to the Grimison model [6] for staggered tubes. All the thermodynamic properties necessary to model the internal heat transfer are computed with look-up tables adopting a fine temperature and pressure discretization.

The Cavallini et al. [5] model adopts a transition criterion that covers all the flow regimes during condensation of pure fluids or azeotropic mixtures. Since this work deals with zeotropic mixtures, the Bell and Ghaly [7] resistance R_a is included in the calculation of the internal heat transfer coefficient $h_{conv,mix}$, as reported in Eq. (2) and (3).

$$h_{conv,mix} = \left(\frac{1}{h_c} + R_a\right)^{-1} \quad (2)$$

$$R_a = x\, c_{p,v} \frac{\Delta T_{gl}}{\Delta H_m} \frac{1}{h_v} \quad (3)$$

The Del Col et al. [8] model is applied to compute the frictional pressure drop of the mixture two-phase flow inside the tubes. The model is an update of the Cavallini model [9] that was developed for mini channels (with diameters lower than 3 mm). However, Cavallini reports that the predictions are also in good agreement with experimental data from macro tubes, showing an average deviation of -7 %. For this reason, the Del Col model is adopted to model pressure drops of the tubes within this work.

In order to solve the heat balance of the various cells in which the rows are discretized, the single domain is also modelled as a cross-flow heat exchanger itself, where the heat exchanged in a single cell is computed accounting for the effectiveness ϵ_{cell} as reported by Navarro and Cabezas-Gómez [10] in Eq. (4) and the maximum heat transferrable.

$$\epsilon_{cell} = 1 - exp\left\{\frac{NTU_{cell}^{0.22}}{CR_{cell}} \cdot \left[exp\left(-CR_{cell} \cdot NTU_{cell}^{0.78}\right) - 1\right]\right\} \quad (4)$$

Based on a preliminary analysis, the layout proposed in Fig. 1 on the left with 7 passes and 7 rows evidenced high pressure drops inside the tube. Balancing the pressure drop and investment costs for the heat exchanger is an optimization topic. Given that the condenser is applied to power cycles for a CSP plant, reducing the pressure drop, thus maximizing cycle efficiency, is more important than minimizing the costs of the condenser as the saving in its capital cost is almost negligible in contrast to the overall CAPEX of the solar power plant. In the preliminary analysis, the layout adopting 3 passes and 7 rows resulted in a three times lower pressure drop than the configuration with 7 passes and 7 rows by splitting the flow in three rows, thus, meeting the requirement for low pressure drops. For this reason, the latter layout is selected as the most promising one.

In the first two passes (six rows), the heat exchange is well driven by the high temperature difference between the working fluid and the air. This enables a reduction of the mass flow rate to a third part (dividing the flow in three rows) reducing the mass velocity inside the single row thus resulting in a lower frictional pressure drop. Given the low velocities and the significant length of the tubes, concentrated pressure drops are within 2 % of the overall pressure drops. In the last pass, instead, where the local temperature difference between the hot and cold side is minimum, the heat transfer is enhanced with a higher mass flow rate at the expense of pressure drops. Finally, the model considers the real condition of non-isothermal mixing between the three rows at the end of the first and second pass.

TABLE 1: CHARACTERISTICS OF TUBES AND FINS.

Parameter	Value
Tube internal / external diameter	20.76 mm / 26.8 mm
Tube disposition	Staggered
Longitudinal / Transversal tube pitch	57.7 mm / 66.7 mm
Fin type	Circular fins
Fin spacing / height	2.52 mm / 15.9 mm
Fin thickness	300 µm
Fin efficiency	77.5%
Area Ratio (external/internal)	27.3
Tube material	Carbon steel
Fin material	Aluminum 1100-annealed

2.2 Thermophysical modelling of CO_2-based mixtures

The CO_2-blends considered in this work are CO_2+R1234ze(E) and CO_2+C_6F_6. The first mixture was considered for the purpose of testing the heat transfer performance during in-tube condensation of a CO_2-rich mixture, while the latter is used in the condenser design since it is one of the most promising working fluids in CSP plants [11].

The thermodynamic characterization of the CO_2+R1234ze(E) mixture was carried out in REFPROP v10 [12] with the GERG-2008 EoS adopting the Kunz and Wagner generalized mixture model (KW0) as mixing rules. The PC-SAFT EoS has been adopted in Aspen Plus V12 [13] for the thermodynamic properties calculation of the CO_2+C_6F_6 mixture; the PC-SAFT parameters of the pure components and the binary interaction parameter optimized on VLE data are taken from literature [11].

Regarding the transport properties assessment, appropriate models were implemented into in-house MATLAB codes due to their relevance into the correlations of both heat transfer and pressure drop. The so-called CO_2-SUPERTRAPP model, a modification of the TRAPP (TRAnsport Property Prediction) method (Ely and Hanley, [14]), has been used for the thermal conductivity of the mixture using carbon dioxide as reference fluid to improve the matching between the CO_2-rich and the reference fluid. The residual thermal conductivity of the pure carbon dioxide has been calculated with a polynomial correlation in temperature and density [15].

As the vapor phase of the two investigated condensing mixtures is characterized by a high molar content of the most volatile component (CO_2), the same approach has been used for the vapor phase viscosity of the mixtures; thus, the so-called CO_2-SUPERTRAPP model has been successfully adopted by Nazeri et al. [16] for CO_2 mixtures with impurities. The excess viscosity of the CO_2 is calculated with the correlation of Fenghour et al. [17]. An Enskog correction term is included in the CO_2-SUPERTRAPP model to account for size differences between the components of the binary mixture.

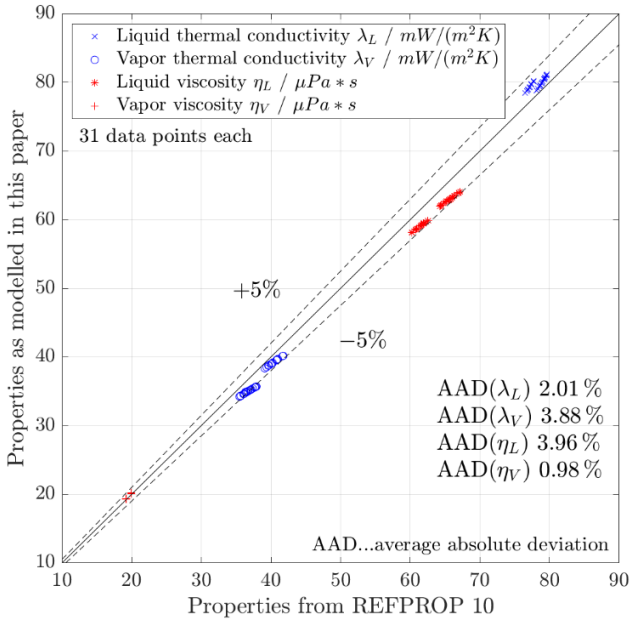

FIGURE 2*:* COMPARISON OF TRANSPORT PROPERTIES FROM REFPROP 10 WITH MODELS PROPOSED BY THE AUTHORS FOR THE CO2+R1234ze(E) MIXTURE.

On the other hand, the viscosity of the mixture's liquid phase has been characterized with the general one-parameter friction theory model of Quiñones-Cisneros et al. [18]. The critical characteristic viscosity of the pure components of the binary mixture, which is a degree of freedom of the f-theory model, is already optimized for pure CO_2 to the value $\eta_{c,CO2}$=376.872 μP. The critical characteristic viscosity of C_6F_6 has been optimized here to the value $\eta_{c,C6F6}$=640.76 μP to fit the experimental liquid viscosities of the pure fluid [19], [20]. The same parameter has been fitted to the value 391.45 μP in the case of R1234ze(E), by a regression of the data of Meng et al. [21]. In addition, appropriate mixing rules are adopted for the mixture. The f-theory model has been applied in conjunction with the PR-EoS to obtain the attractive and repulsive pressure contributions.

Considering that GERG-2008 has an accurate $P-\rho-T$ characterization of the mixture CO_2+R1234ze(E), high accuracy is expected in its exact shape factor approach in the transport properties modelling; therefore, it is used for the validation of the local HTC in chapter 2.3. Regarding the CO_2+R1234ze(E) mixture, in all the thermodynamic conditions of the experimental HTC validation, the in-house code for transport properties results in good accordance with REFPROP, as can be noticed from the absolute deviations represented in Fig. 2.

2.3 Solutions to enhance heat transfer

An efficient way to improve the heat transfer coefficient, and thus to reduce the heat exchanger area, consists of the adoption of corrugated surfaces to improve the flow turbulence. In this paper, a tube with internal microfins and groovy fins on the air side is proposed and presented in Fig. 3 to enhance the heat transfer while condensing a CO_2-based mixture. In comparison, the smooth tube with outer circular fins can be seen on the left side.

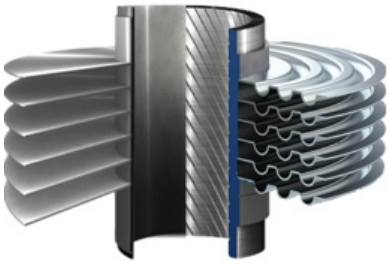

FIGURE 3: LEFT: TUBE WITH CIRCULAR FINS, RIGHT: ENHANCED TUBE WITH MICROFINS AND GROOVY FINS.

Microfins for inside tube condensation have been studied intensively in the last 15 years as they can increase the heat transfer by a factor of 1.5-3.2 compared to the smooth tube [22]. As a consequence, the internal pressure drops are enhanced too, by a factor between 1.1 and 1.7, depending on the microfins geometry. The DIESTA tube is a microfinned tube specifically developed for cooling and condensation of working fluids with a tube diameter suitable for industrial applications. Dedicated internal grooves have been investigated and chosen for the condensation of CO_2-based mixtures, resulting in the product *DIESTA CO2 SC1*.

For the first step of the validation, results presented in Chapter 4.2, circular fins and smooth internal tube surfaces are assumed. For the proposed full-scale condenser, shown in Chapter 4.3, the DIESTA tube is instead combined with the patented groovy fins on the air side. The groovy fin technology had been developed for air-cooled condensers and relies on two effects: increasing turbulence and reducing stagnation zones downstream the tubes by guiding the air. For these two reasons,

the heat transfer on the external side is enhanced up to 20 % at constant fan power. The air-side pressure losses are also raised by a factor around 1.12 at constant air face velocity.

The calculation of heat transfer and pressure drops is carried out by using proprietary enhancement factors with respect to the model for smooth fins and tubes.

2.4 Case study: Condensation of the CO_2+C_6F_6 mixture

In this paper, the design of the air-cooled condenser is carried out for CO_2+C_6F_6 mixture with 92% molar (75% mass) fraction of carbon dioxide thus leading to a critical point at 76 °C and 123 bar, presented in Fig. 4. The cycle layout of the case study is a simple recuperated cycle working in a temperature range between 51 °C and 550 °C. The assumptions on the non-idealities of the components are taken from literature [11]. Even if the selected molar composition is not the one that guarantees the maximum efficiency of the associated transcritical power cycle [11], it is adopted mainly for two reasons: i) ensure full condensation at 51 °C in conditions sufficiently distant from the critical point; ii) minimize the C_6F_6 content to avoid material and degradation issues, reduce the environmental impact and the cost of the working fluid.

The simple recuperated transcritical cycle is characterized by a single-phase regeneration, so that the flow enters the condenser at the dew point, avoiding maldistribution issues in the condenser headers and in the piping between the condenser and the recuperator.

As shown in the PT-envelope in Fig. 4, an increase of CO_2 content entails a reduction of the dew-point temperature: the hot-end of the recuperator gets close to the pump outlet temperature, so the cycle efficiency increases significantly. On the other hand, a CO_2 molar content higher than 92% leads to a condensation process too close to the critical point. Thus, the selected mole fraction represents a good compromise.

The mass flow rate considered for the case-study is equal to 1200 kg/s, a value that guarantees a cycle net electrical output around 100 MW_{el}.

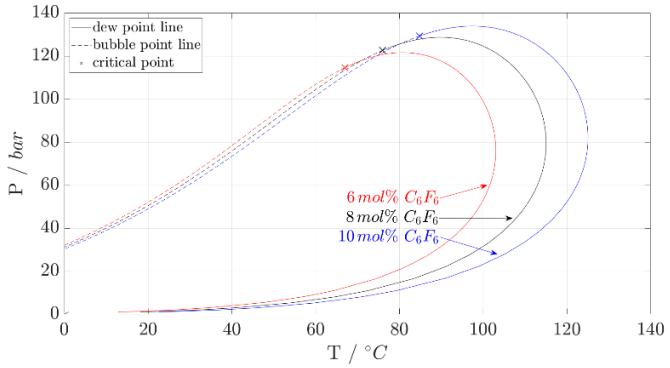

FIGURE 4*:* PT-DIAGRAM OF THREE COMPOSITIONS OF THE MIXTURE CO_2+C_6F_6.

3. VALIDATION

3.1 Validation of inner heat transfer correlation via experimental data

An overall lack of experimental data of HTC in the two-phase region for CO_2-based condensing mixtures is evidenced in literature: for this reason, it is not easy to find reliable references which indicate a solid correlation within a certain accuracy for designing the condenser of a CO_2-based cycle.

In this chapter, the heat transfer correlation presented in Chapter 2.1 is validated against experimental data taken within this work of the CO_2+R1234ze(E) mixture during condensation at the conditions summarized in Tab. 2. This mixture was selected for the experimental campaign as it is basically non-hazardous but can be treated as a zeotropic CO_2-based mixture with a fluorinated compound. In contrast, C_6F_6 is flammable and slightly toxic[2]. Even if R1234ze(E) does not suit the proposed application as it is not stable at elevated temperatures, it was very important to assess the heat transfer behavior of a CO_2-based mixture to choose correct models for condenser designs as no relevant literature data are available on condensing flows of CO_2-based mixtures.

TABLE 2: CONDITIONS OF HTC-VALIDATION EXPERIMENTS.

Conditions	value
Pressure / bar	63; 66
Working fluid	CO_2+ R1234ze(E)
Mass velocity $G\ /kgm^{-2}s^{-1}$	277; 554; 831
Mass fraction CO2 / %	87
Mass fraction R1234ze(E) / %	13
Vapor fraction	0-0.8

The experiments were performed at a test facility at TU Wien with a horizontal tube-in-tube heat exchanger, the so-called test-tube, shown in Fig. 5 and 6. It is operated in counterflow configuration with working fluid on the inside and cooled by water in the annulus. The geometrical parameters are summarized in Tab. 3.

TABLE 3: PARAMETERS OF THE TEST-TUBE.

Parameter	value
Tube internal diameter $d_{int}\ /\ mm$	21.784
Tube external diameter $d_{ext}\ /\ mm$	25.400
Heat exchanger section length $/\ mm$	1033.7
Section II-III length $l\ /\ mm$	333
Steel type	SA-179
Steel thermal conductivity $\lambda_{steel}\ /\ Wm^{-1}K^{-1}$	60

The following measurement devices are installed on the working fluid side: mass flow $\dot{m}$ (Coriolis sensor) and pressure p (piezoresistive) in piping before test-tube, working fluid bulk temperature T_b at the middle of test-tube. On the water side, temperature $T_{H2O,in}$ and pressure p are measured at the inlet, and

[2] Heat transfer measurements with CO_2+C_6F_6 are planned in 2023.

volume flow $\dot{V}_{H2O}$ and temperature $T_{H2O,out}$ at the outlet. Water temperature in the annulus is measured at position II and III (Pos. II, Pos. III). Moreover, at Pos. II and III, the outer wall temperature of the inner tube is measured at three radial positions as can be seen in the cross section in Fig. 7. Temperature sensors are PT100 of class A or AA, see Tab. 4.

TABLE 4: *TEMPERATURE MEASUREMENT UNCERTAINTY CLASS OF PT100.*

Sensors	Uncertainty
$T_{bulk}, T_w, T_{H2O,1}, T_{H2O,2}$	Class AA
$T_{H2O,in}, T_{H2O,out}$	Class A

The section between position II and III is used to calculate a pseudo-local heat transfer coefficient on the CO_2 side.
From the water side, the heat flux is calculated as shown in Eq. (5), using water properties modelled after IAPWS [23]:

$$\dot{q} = \frac{\dot{Q}}{\pi d_i l} = \frac{\dot{V}_{H2O,out} * \rho_{H2O,out}(h_{H2O,nout} - h_{H2O,in})}{\pi d_i l} \quad (5)$$

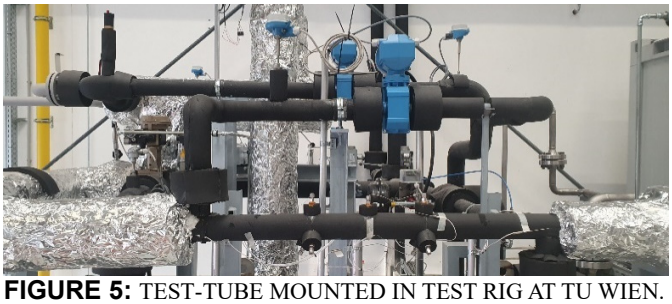

FIGURE 5: TEST-TUBE MOUNTED IN TEST RIG AT TU WIEN.

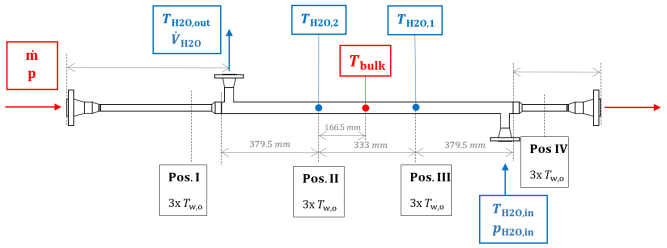

FIGURE 6: SKETCH OF TEST-TUBE AND SENSORS' POSITION; RED: WORKING FLUID, BLUE: WATER, BLACK: WALL TEMPERATURE.

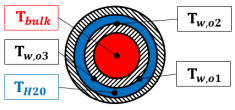

FIGURE 7: POSITION OF TEMPERATURE SENSORS AT THE CROSS SECTION OF THE TEST-TUBE.

The outer wall temperature in the section II-III is assumed nearly constant due to axial heat conduction and the short distance between II and III and therefore calculates as a mean of the wall temperatures at position II $T_{w,o,II}$ and III $T_{w,o,III}$.

Under the assumption of one-dimensional heat conduction through the tube, the inner wall temperature in section II-III can be calculated as:

$$T_{w,int} = T_{w,ext} + \dot{Q} \frac{ln(d_{ext} - d_{int})}{2\pi l \lambda_{steel}} \quad (6)$$

The experimental local heat transfer coefficient is then with the above mentioned assumptions calculated as:

$$h_{loc} = \frac{\dot{q}}{T_{w,int} - T_b} \quad (7)$$

Where T_b is the measured temperature of the working fluid at the middle of the test-tube.

The types of measurement equipment and their uncertainties according to the suppliers are reported in Tab. 5. The error analysis on the experimental heat transfer coefficient was executed by propagation of uncertainty of the measured values:

$$\Delta h_{loc} = \sqrt{\left(\frac{\partial h_{loc}}{\partial T_{w,ext}}\right)^2 * \Delta T_{w,ext}^2 + \left(\frac{\partial h_{loc}}{\partial T_b}\right)^2 * \Delta T_b^2 + \left(\frac{\partial h_{loc}}{\partial \dot{Q}}\right)^2 * \sigma_{\dot{Q}}^2} \quad (8)$$

The standard deviation of the transferred heat, $\sigma_{\dot{Q}}$, was obtained by measurements with pure CO_2 where the heat balance on both sides, CO_2 and water, could be used as additional information to reduce the uncertainty of the data. The pressure dependability of density was neglected when analyzing the volume flow of water. The influence of the reference temperature on the analog-to-digital (A/D) converters was neglected as the control cabinet is in an indoor air-conditioned environment.

For the calculated heat transfer measurements the error propagation was only executed for measured input data as there is a lack of data on the uncertainty of the used property models. Therefore, the uncertainties of the calculated HTC has to be seen as a minimum uncertainty.

TABLE 5: UNCERTAINTY OF INPUTS TO CORRELATION-CALCULATED AND EXPERIMENTAL HTC.

	Type	Uncertainty
$\dot{m}_{wf}$	Endress&Hauser, Proline Promass G 100	0.15 % for liquid
$\dot{V}_{H2O}$	Endress&Hauser, Promag 10E25 and 10E32	0.5 % + 2 mm/s
P	ICCP Messtechnik, PCE-28	0.2 %
$T_{class\ AA}$	TC Direct, PT100	0.1 + 0.0017*T(°C)
$T_{class\ A}$	WIKA TR10-H and Endress& Hauser TR88	0.15 + 0.002*T(°C)
A/D converter for $\dot{V}$	B&R, AI4622, electric current	Gain 0.1%, Offset 0.16%
A/D converter for P	B&R, AI4632, electric current	Gain 0.08 %, Offset 0.02 %
A/D converter for T	B&R, ATB312	Gain 0.0059 %, Offset 0.0015 %

3.2 Validation of the proposed model against commercial software from HTRI

The overall model is validated by comparison with the widely used commercial software Xace® by the Heat Transfer Research Incorporation HTRI. The results from this program are considered as a standard within the community and allow for rating, simulation and design. The models of heat transfer and pressure drop in Xace® rely on HTRI research-based methods, ESCOA methods or correlations developed by the user.

The main differences between the here presented MATLAB model and Xace® (mode: rating) are the inputs and outputs as shown in Tab. 6.

TABLE 6: COMPARISON OF THE INPUTS (I) AND OUTPUTS (O) OF THE MODELS.

Parameter	MATLAB	Xace®
Heat duty	I	I
Hot side mass flow rate	I	I
Hot side temperature range	I	I
Geometry (except tube length)	I	I
Length of tubes	O	I
Number of tubes	O	I
Air face velocity	I	I
Air inlet temperature	I	I
Air outlet temperature	O	O
Hot side pressure drop	I	O
Heat transfer coefficients	O	O

4. RESULTS AND DISCUSSION

4.1 Validation of heat transfer correlation

A validation of the models used for the HTC calculation presented in Chapter 2.1 is carried out with the experimental data of the CO_2+R1234ze(E). As presented in Fig. 8, the experiments seem satisfactory for the comparison of heat transfer coefficients as uncertainties of the experimental HTC are very low with ±12.6 W/(m²K) on average and calculated ones lie within ±68.4 W/(m²K).

The experimental HTCs of the CO_2+R1234ze(E) mixture fit very well with the ones calculated by Cavallini [5] corrected by the Bell-Ghaly [7] approach: the majority of the data points lie within a range of ±10 %.

The heat transfer coefficients were predicted with an average absolute deviation of 5.34 % and a standard deviation of 0.98 % which is very well within the reported range of other author´s results. For the lower vapor quality conditions, the model seems to overestimate the HTC, and vice versa. This might suggest the necessity of a more sophisticated correction factor. However, the authors consider the prediction satisfactory for the implementation in the MATLAB code.

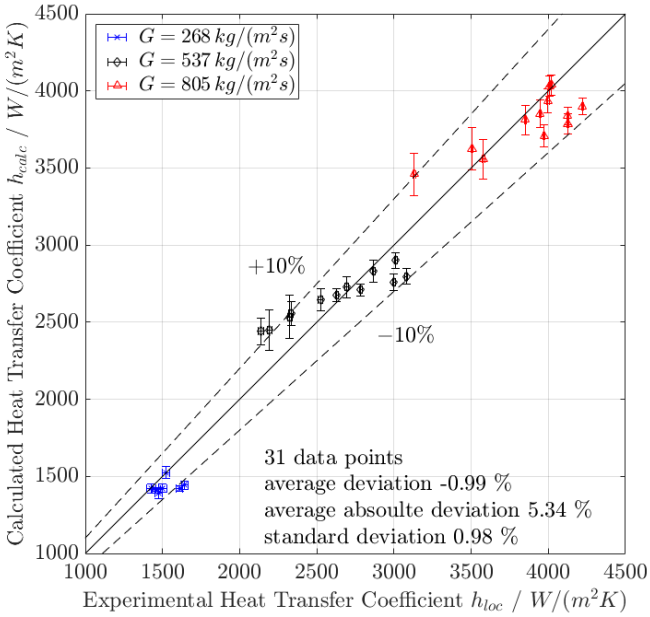

FIGURE 8: COMPARISON OF EXPERIMENTAL TO CALCULATED HEAT TRANSFER COEFFICIENTS OF THE MIXTURE CO_2+R1234ze(E).

4.2 Validation of the proposed model - CO_2+C_6F_6 case study (without enhanced heat transfer)

As a preliminary step to the presentation and discussion of the design of the full condenser, a comparison between the in-house MATLAB code and the result from Xace® is carried out for the case study and the selected tube configuration with 7 rows and 3 passes of Fig. 1. The calculations proposed in this section are carried out assuming circular fins and smooth internal tube surfaces, as described in Chapter 2.3, not enhancing the heat transfer coefficient with groovy fins and internal microfins.

The air side boundary conditions are selected according to the values suggested in Xace®, representative of a good match between the design of the fans and the tubes: the air face velocity is hence set at 3.23 m/s and a design air side temperature difference of 23 °C is imposed. The simulations performed in MATLAB assume these values as reference, increasing the air temperature difference in case a lower heat transfer area (and therefore air passage area) is computed, to enforce the air side mass conservation equation. This choice allows the reduction of air mass flow rate for condensers with enhanced heat transfer at constant air face velocity, hence reducing the air side pressure drops and the auxiliary consumption.

In the MATLAB calculations, the pressure drop on the hot side is set below 0.5 bar, since the design aims at representing a condenser with an overall pressure drop below 1 bar including the additional pressure drops in the headers and in the piping.
The results, presented in Tab. 7, show an excellent agreement between the two models, presenting almost negligible variations.

The relative deviation on the computed area is only around 2.3 %. Nevertheless, the higher deviation in tube length (around 5.4 %) and number of tubes (around 9.5 %) evidences the effect

of the different HTC and pressure drop models: as a matter of fact, the two effects are almost balanced between each other and their opposite contributions tend to make the results comparable, since the relative error on the area is well below the one on tube length and number of tubes.

TABLE 7: COMPARISON OF INPUTS AND RESULTS OF THE MODEL FROM THIS WORK AND COMMERCIAL SOFTWARE.

Parameter	MATLAB	Xace®
Heat duty	236 MW	
Mixture mass flow	1200 kg/s	
Air inlet temperature	36 °C	
Mixture temperature	From 114 °C to 51 °C	
Air face velocity	3.23 m/s	
Hot side pressure drop	0.46 bar	
Air outlet temperature	59.5 °C	59 °C
Number of tubes	2030	2242
Length of the tube	135 m	128.1 m
Length of the pass	19.3 m	18.3 m
External HX area	487 800 m^2	499 500 m^2
Overall HTC	23.0 $W/m^2/K$	21.6 $W/m^2/K$

4.3 Full scale heat exchanger for CO_2+C_6F_6 with enhanced heat transfer

As the design of the condenser with smooth fins and tubes has been carried out and compared with Xace® results, an enhanced configuration with groovy fins and DIESTA tubes is presented along with a detailed characterization of the temperature and heat distribution along the tube.

As a matter of fact, in this configuration the ratio between the convective heat transfer coefficients on the hot side and air side is a value close to the area ratio reported in Tab. 1 (about 27): for this reason, improving the internal heat transfer coefficient is as important as improving the external one, and the two coefficients have the same relative importance in determining the overall HTC.

The resulting design is presented in Tab. 8, modelled in MATLAB assuming the same tube configuration and boundary conditions reported in Tab. 7. In this configuration, the additional internal microfins and external groovy fins decrease the heat transfer area by around 14% and the pass length by 23% since a lower tube length is necessary to limit the pressure drop on the hot side, thus, requiring a slightly higher number of tubes (+11 %).

In addition, the temperature distribution along the seven rows is depicted in Fig. 9 and 10 both for the air side and the mixture side, along with the thermal power and HTC of Fig. 11 and 12, respectively. From the results it is possible to notice that the heat exchanged and the temperature of the hot flow are not homogeneously distributed along the three rows of each passes, while the air temperature at the outlet of the condenser will be much higher at the hot end of the condenser. In particular, the higher heat exchange occurs in the row where the air temperature is lower, as the hot side mass flow rate is evenly distributed in the various rows. The overall HTC, instead, is higher in the last row due to the higher internal mass flow rate, while it increases slightly along the previous two passes due to the increase of working fluid velocity. Ultimately, the reduction of air mass flow rate is proportional to the increment in air temperature difference (around 15 %). This effect can help reducing the auxiliary fan consumption with respect to the reference case, which would otherwise increase due to the presence of the groovy fins.

TABLE 8: COMPARISON OF RESULTS WITH AND WITHOUT HEAT TRANSFER ENHANCEMENT.

Parameter	Without enhancement	With enhancement
Model	MATLAB	MATLAB
Type of fins	Circular	Groovy
Type of tubes	Smooth	Microfins
Air outlet temperature	59.5 °C	63.1 °C
Number of tubes	2030	2250
Length of the tube	135 m	104.2 m
Length of the pass	19.3 m	14.9 m
External HX area	487800 m^2	417300 m^2
Overall HTC	23.0 $W/m^2/K$	28.8 $W/m^2/K$

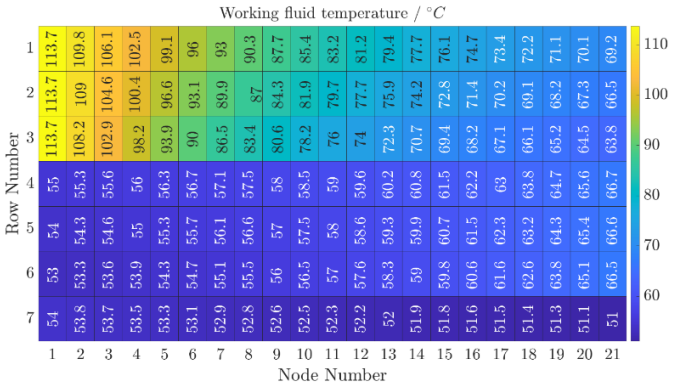

FIGURE 9: WORKING FLUID TEMPERATURE IN °C.

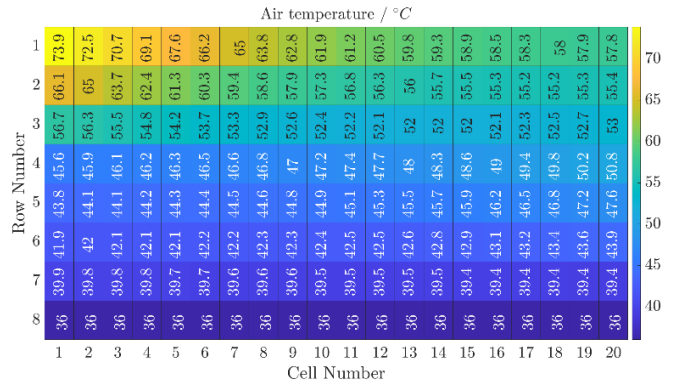

FIGURE 10: AIR TEMPERATURE IN °C.

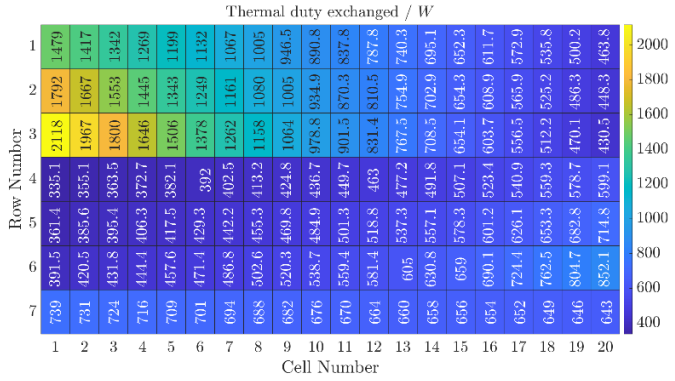

FIGURE 11: THERMAL DUTY EXCHANGED IN W.

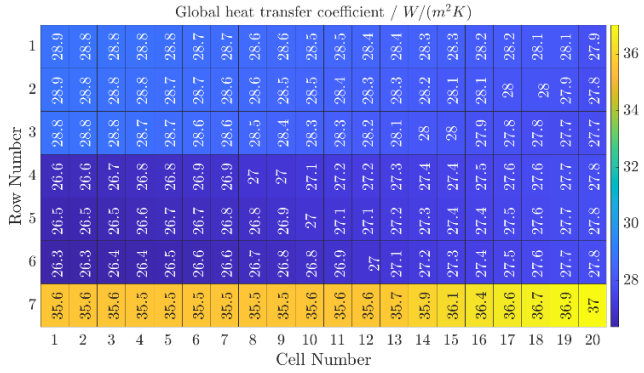

FIGURE 12: GLOBAL HTC IN W/m²/K.

4.4 Comparison of a pure CO_2 and a CO_2-based mixture heat exchanger

Finally, the heat exchanger with groovy fins and internal microfins is also adopted and designed for the heat rejection unit of a pure sCO_2 power cycle, representative of an advanced cycle for CSP applications.

In case of pure CO_2, the flow does not condense and the Gnielinski correlation [24], a widely renowned correlation for single phase in-tube heat transfer coefficient, is adopted. The thermodynamic and transport properties of the CO_2 are computed with the Span and Wagner EoS [25]. The boundary conditions of the CO_2 configuration are presented in Tab. 9 along with the resulting design. In order to properly compare the two heat exchangers, the same heat duty, internal pressure drop and temperature difference on the hot and cold side are assumed. Due to the different thermodynamic properties and the fixed heat duty, the mass flow rate is also different, while the pressure of the CO_2 cooler is set to 100 bar as this is an optimum value for sCO_2 cycles with minimum temperatures around 50 °C [26].

The results show a higher number of tubes and a lower tube length for the sCO_2 cooler to meet the same pressure drop. As the local working fluid velocity in case of pure sCO_2 is higher than the one of the mixture, a higher frictional pressure drop per unit length is computed. On the other hand, sCO_2 is characterized by a better heat exchange performance thanks to its low viscosity that entails high local Reynolds and Nusselt numbers. The heat transfer performance of the pure CO_2 increases towards low temperatures, closer to the critical point, due to a marked increase of the thermal conductivity. The opposite trend is noted in the heat transfer performance of the mixture, which decreases during condensation. At almost the same mass flow in the single tube, the improved heat exchange capability and the higher frictional pressure drop in case of pure CO_2 entail a lower tube length to meet the same pressure drop.

TABLE 9: *COMPARISON OF DESIGNS FOR PURE CO_2 AND THE CO_2+C_6F_6 MIXTURE.*

Parameter	Pure CO_2	CO_2+C_6F_6 mixture
Heat duty	236 MW	
Hot side mass flow	1749 kg/s	1200 kg/s
Hot side pressure	100 bar	92 bar
Air inlet temperature	36 °C	
Hot side temperature	From 114 °C to 51 °C	
Air face velocity	3.23 m/s	
Pressure drop	0.46 bar	
Air outlet temperature	65.4 °C	63.1 °C
Number of tubes	3055	2250
Length of the tube	70.2 m	104.2 m
Length of the pass	10.0 m	14.9 m
External HX area	381 700 m²	417 300 m²
Overall HTC	28.6 W/m²/K	28.8 W/m²/K

In conclusion, the heat exchange area is reduced for the sCO_2 configuration by 8% with respect to the mixture, although a slightly lower overall HTC is computed. The reason for this counterintuitive result lies in the average temperature difference between the air and the hot flows, being higher in the sCO_2 case than in the mixture.

Figure 13 and 14 depict the heat transfer in the sCO_2 cooler and the deviation in hot and cold temperature difference between the sCO_2 case and the CO_2+C_6F_6 case, which generally is higher for the sCO_2 by up to 5 K, depending on the cell position.

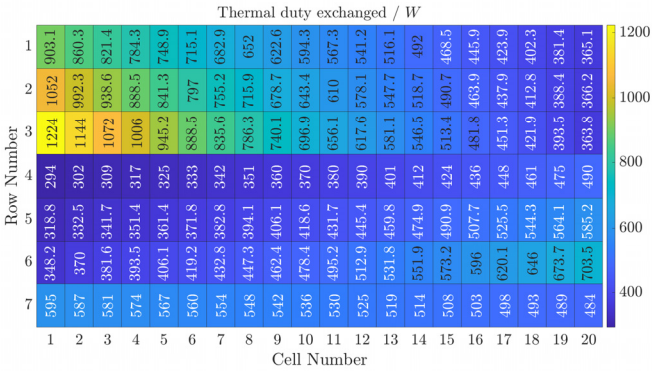

FIGURE 13: THERMAL DUTY EXCHANGED IN W FOR PURE CO_2.

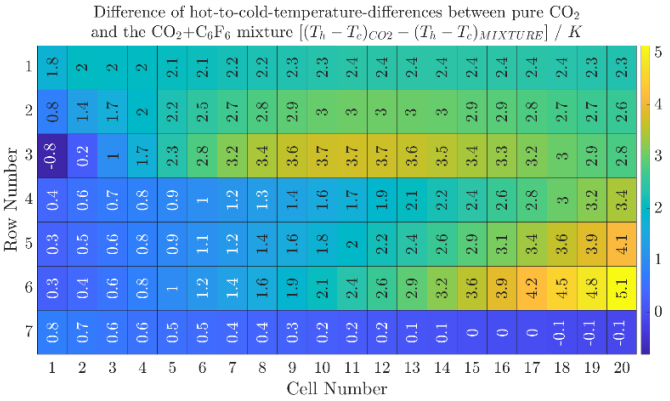

FIGURE 14: DIFFERENCE OF HOT-TO-COLD-TEMPERATURE DIFFERENCES IN K FOR PURE CO_2 AND THE MIXTURE.

4. CONCLUSION

In this work, a finite volume model for the design of air-cooled condensers of mixtures is presented and validated against the commercial software Xace® by HTRI, showing very good agreement. Dedicated models of heat transfer coefficients, the Cavallini model [5] and the Bell and Ghaly approach [7], and transport properties for condensing mixtures are adopted and validated experimentally on the CO_2+R1234ze(E) mixture, highlighting the novel approach in the condenser design with innovative mixtures. Finally, an enhanced tube configuration with microfins and groovy fins on the airside is presented and the performance improvements are evidenced.

Being the heat transfer performances of condensing mixtures generally considered slightly poorer than supercritical fluids, future works will aim at including economic evaluations of the increment in heat exchangers size in the techno-economic comparisons of these two power cycle technologies, along with the respective increment in cycle efficiency that some CO_2-based mixtures present with respect to pure CO_2 in power cycles.

ACKNOWLEDGEMENTS

The authors thank Dario Alfani for providing the basic structure of the heat exchanger model and his contribution during the review process and proof-reading.

The SCARABEUS project has received funding from European Union's Horizon 2020 research program under grant agreement N°814985.

REFERENCES

[1] F. Crespi, D. Sánchez, J. Rodríguez and G. Gavagnin, "A thermo-economic methodology to select sCO2 power cycles for CSP applications".*Renewable Energy.* https://doi.org/10.1016/j.renene.2018.08.023.

[2] G. Manzolini, M. Binotti, D. Bonalumim, C. Invernizzi and P. Iora, "CO2 mixtures as innovative working fluid in power cycles applied to solar plants. Techno-economic assessment," *Solar Energy,* pp. 530-544, 2019. https://doi.org/10.1016/j.solener.2019.01.015.

[3] F. Crespi, P. R. de Arriba, D. Sánchez and A. Muñoz, "Preliminary investigation on the adoption of CO2-SO2 working mixtures in a transcritical Recompression cycle," *Applied Thermal Engineering,* March 2022. https://doi.org/10.1016/j.applthermaleng.2022.118384.

[4] E. Morosini, A. Ayub, G. di Marcoberardino, C. M. Invernizzi, P. Iora and G. Manzolini, "Adoption of the CO2 + SO2 mixture as working fluid for transcritical cycles: A thermodynamic assessment with optimized equation of state," *Energy Conversion and Management,* vol. 255, 2022. https://doi.org/10.1016/j.enconman.2022.115263.

[5] A. Cavallini, D. Del Col, L. Doretti, M. Matkovic, L. Rossetto, C. Zilio and G. Censi, "Condensation in Horizontal Smooth Tubes: A New Heat Transfer Model for Heat Exchanger Design," *Heat Transfer Engineering,* pp. 31-38, 2006.

[6] F. P. Incropera, D. P. DeWitt, T. L. Bergman, A. S. Lavine and et al., Fundamentals of heat and mass transfer, vol. 6, New York: Wiley, 1996.

[7] K. J. Bell and M. A. Ghaly, "An Approximate Generalized Design Method for Multicomponent/Partial Condenser," *AIChESymp. Ser.,* vol. 69, pp. 72-79, 1973.

[8] D. Del Col, A. Bisetto, M. Bortolato, D. Torresin and L. Rossetto, "Experiments and updated model for two phase frictional pressure drop inside minichannels," *International Journal of Heat and Mass Transfer,* pp. 326-337, 2013. https://doi.org/10.1016/j.ijheatmasstransfer.2013.07.093.

[9] A. Cavallini, D. Del Col, M. Matkovic and L. Rossetto, "Frictional pressure drop during vapour–liquid flow in minichannels: Modelling and experimental evaluation," *International Journal of Heat and Fluid Flow,* no. 1, pp. 131-139, 2009. https://doi.org/10.1016/j.ijheatfluidflow.2008.09.003.

[10] H. Navarro and L. Cabezas-Gómez, "Effectiveness-ntu computation with a mathematical model for cross-flow heat exchangers," *Brazilian Journal of Chemical Engineering,* p. 509–521, 2007.

[11] G. Di Marcoberardino, E. Morosini and G. Manzolini, "Preliminary investigation of the influence of equations of state on the performance of CO2 + C6F6 as innovative working fluid in transcritical cycles," *Energy,* Vols. 238, Part B, 2022. https://doi.org/10.1016/j.energy.2021.121815.

[12] E. Lemmon, I. Bell, M. Huber and M. McLinden, *NIST Standard Reference Database 23: Reference Fluid Thermodynamic and Transport Properties-REFPROP, Version 10.0, National Institute of Standards and Technology, Standard Reference Data Program,* Gaithersburg, 2018.

[13] I. Aspen Technology, *Aspen Plus (R), Version V12.1,* 2021.

[14] J. F. Ely and H. J. M. Hanley, “Prediction of Transport Properties,” *Industrial & engineering chemistry fundamentals,* vol. 20 (4), p. p.323, 1981.

[15] M. L. Huber, E. A. Sykioti, M. J. Assael and R. A. Perkins, "Reference Correlation of the Termal Conductivity of Carbon Dioxide from the Triple Point to 1100 K and up to 200 MPa," *J. Phys. Chem. Ref. Data,* 2016. https://doi.org/10.1063/1.4940892.

[16] M. Nazeri, A. Chapoy, R. Burgass and B. Tohidi, "Viscosity of CO2-rich mixtures from 243 K to 423 K at pressures up to 155 MPa: New experimental viscosity data and modelling,," pp. 100-114, 2018. https://doi.org/10.1016/j.jct.2017.11.005.

[17] A. Fenghour, W. A. Wakeham and V. Vesovic, "The Viscosity of Carbon Dioxide," *Journal of Physical and Chemical Reference Data,* no. 31, 1998. https://doi.org/10.1063/1.556013.

[18] S. E. Quiñones-Cisneros, C. K. Zéberg-Mikkelsen and E. H. Stenby, "One parameter friction theory models for viscosity," *Fluid Phase Equilibria,* no. 1-2, pp. 1-16, 2001. https://doi.org/10.1016/S0378-3812(00)00474-X.

[19] M. G. Freire, A. G. M. Ferreira, I. M. A. Fonseca, I. M. Marrucho and J. Coutinho, "Viscosities of Liquid Fluorocompounds," *J. Chem. Eng. Data,* pp. 538-542, 2008. https://doi.org/10.1021/je700632z.

[20] J. H. Dymond, J. Robertson and J. D. Isdale, "Transport properties of nonelectrolyte liquid mixtures—IV. Viscosity coefficients for benzene, perdeuterobenzene, hexafluorobenzene, and an equimolar mixture of benzene + hexafluorobenzene from 25 to 100°c at pressures up to the freezing pressure," *International Journal of Thermophysics,* p. pages 223–236, 1981.

[21] X. Meng, G. Qiu, J. Wu and I. M. Abdulagatov, "Viscosity measurements for 2,3,3,3-tetrafluoroprop-1-ene (R1234yf) and trans-1,3,3,3-tetrafluoropropene (R1234ze(E))," *The Journal of Chemical Thermodynamics,* pp. 24-30, 2013. https://doi.org/10.1016/j.jct.2013.03.013.

[22] Z. Wu, B. Sundén, V. V. Wadekar and W. Li, “Heat Transfer Correlations for Single-Phase Flow, Condensation, and Boiling in Microfin Tubes,” *Heat Transfer Engineering,* no. 36:6, pp. 582-595, 2015. https://doi.org/10.1080/01457632.2014.939531.

[23] International Association for the Properties of Water and Steam, IAPWS R6-95(2018), "Revised Release on the IAPWS Formulation 1995 for the Thermodynamic Properties of Ordinary," 2018.

[24] V. Gnielinski, "New equations for heat and mass transfer in the turbulent flow in pipes and channels," *(Jahrestreffen der Verfahrensingenieure, Berlin, West Germany, Oct. 2-4, 1973.) Forschung im Ingenieurwesen,* vol. 1, pp. 8-16, 1975.

[25] R. Span and W. Wagner, "A New Equation of State for Carbon Dioxide Covering the Fluid Region from the Triple-Point Temperature to 1100 K at Pressures up to 800 MPa," *Journal of Physical and Chemical Reference Data,* 1996. https://doi.org/10.1063/1.555991.

[26] M. Binotti, C. M. Invernizzi, P. Iora and G. Manzolini, "Dinitrogen tetroxide and carbon dioxide mixtures as working fluids in solar tower plants," *Solar Energy,* pp. 203-213, 2019. https://doi.org/10.1016/j.solener.2019.01.079.